



## Highly active poly(3-hexylthiophene) nanostructures for photocatalysis under solar light



Dita Floresyona<sup>a</sup>, Fabrice Goubard<sup>b</sup>, Pierre-Henri Aubert<sup>b</sup>, Isabelle Lampre<sup>a</sup>, Jérémie Mathurin<sup>a</sup>, Alexandre Dazzi<sup>a</sup>, Srabanti Ghosh<sup>a,1</sup>, Patricia Beaunier<sup>c</sup>, François Brisset<sup>d</sup>, Samy Remita<sup>a,e</sup>, Laurence Ramos<sup>f</sup>, Hynd Remita<sup>a,g,\*</sup>

<sup>a</sup> Laboratoire de Chimie Physique, UMR 8000 CNRS, Université Paris-Sud, Université Paris-Saclay, 91405 Orsay, France

<sup>b</sup> Laboratoire de Physicochimie des Polymères et des Interfaces (LPPI, EA 2528), Université de Cergy-Pontoise, 5 mail Gay Lussac, F-95031 Neuville-sur-Oise Cedex, France

<sup>c</sup> Sorbonne Université, UPMC Univ Paris 06, CNRS, UMR 7197, Laboratoire de Réactivité de Surface, F-75005 Paris, France

<sup>d</sup> Institut de Chimie Moléculaire et des Matériaux d'Orsay, ICMMO, UMR 8182 CNRS, Université Paris-Sud, Université Paris Saclay, Bât 410-420, Orsay F-91405, France

<sup>e</sup> Département CASER, Ecole SITI, Conservatoire National des Arts et Métiers, CNAM, 292 rue Saint-Martin, 75141 Paris Cedex 03, France

<sup>f</sup> Laboratoire Charles Coulomb (L2C) UMR 5221 CNRS-Université de Montpellier, 34095 Montpellier, France

<sup>g</sup> CNRS, Laboratoire de Chimie Physique, UMR 8000, 91405 Orsay, France

### ARTICLE INFO

#### Article history:

Received 7 December 2016

Received in revised form 6 February 2017

Accepted 21 February 2017

Available online 22 February 2017

#### Keywords:

Poly(3-hexylthiophene)

Conjugated polymer nanostructures

Photocatalysis

Superoxide radical

Water treatment

### ABSTRACT

Conjugated polymer nanostructures have recently emerged as a new class of very active photocatalysts under solar light. Poly(3-hexylthiophene) (P3HT) is one of the commonly used conjugated polymers for photovoltaics applications. P3HT nanostructures synthesized in soft templates provided by hexagonal mesophases show high photocatalytic activity for degradation of pollutants under both UV and visible light. These photocatalysts are very stable even after repeated cycling. Addition of scavengers and mechanistic studies show that  $O_2^{\bullet-}$  is the main radical responsible for degradation of phenol taken as a model pollutant. P3HT nanostructures can be easily deposited on flat supports such as quartz for photocatalytic applications avoiding a separation step by centrifugation. Most interestingly, the photocatalytic activity of these P3HT nanostructures is highly enhanced when they are supported on a solid surface opening new perspectives in photocatalytic reactors and self-cleaning surfaces.

© 2017 Elsevier B.V. All rights reserved.

### 1. Introduction

Titanium dioxide ( $TiO_2$ ) is the most commonly used semiconductor for photocatalysis because of its low price, high stability and non-toxicity. However,  $TiO_2$  is only active under UV light irradiation (band gap > 3.2 eV for anatase and 3.0 eV for rutile), while solar light consists of only 4% of UV light. Doping or modification of  $TiO_2$  to enhance its photocatalytic activity under solar light is therefore a very active field of research [1–7]. Furthermore, to avoid filtration difficulties, an immobilization of the photocatalyst is necessary. For application of titania in air and water depollution, many works have focused on the deposition and immobilization of  $TiO_2$  on different

supports such as glass beads or plates, on a non-woven glass fiber fabric, steel, or on porous materials, avoiding the separation step of the titania powder. Whatever the support, the immobilization of titania lowers in general its photoactivity because of the difficulty for the UV photons to reach a part of the solid [8]. The search for new photocatalytic materials, which are active under solar light, and mainly under visible light has therefore received a lot of attention in the last decade [9–13].

With the discovery of conductive polyacetylene in 1978, conducting polymers (CPs) have received significant interest from both scientific and engineering communities [14]. The combination between the superior electronic properties of semiconductors (such as high conductivity, mechanical and thermal stability) and the advantages of organic materials (low cost and easy processing) render CPs promising materials for a variety of optoelectronic applications such as solar cells, light emitting diode, field-effect transistors, etc [15–20]. Among conductive conjugated polymers, poly(alkylthiophenes) have emerged as one of the most popular class. Poly(3-hexylthiophene) (P3HT) is an organic semiconduc-

\* Corresponding author at: Laboratoire de Chimie Physique, UMR 8000 CNRS, Université Paris-Sud, Université Paris-Saclay, 91405 Orsay, France.

E-mail address: [hynd.remita@u-psud.fr](mailto:hynd.remita@u-psud.fr) (H. Remita).

<sup>1</sup> Present address: Department of Chemical, Biological and Macromolecular Sciences, S. N. Bose National Centre for Basic Sciences, Block JD, Sector III, Salt Lake, Kolkata 700 098, India

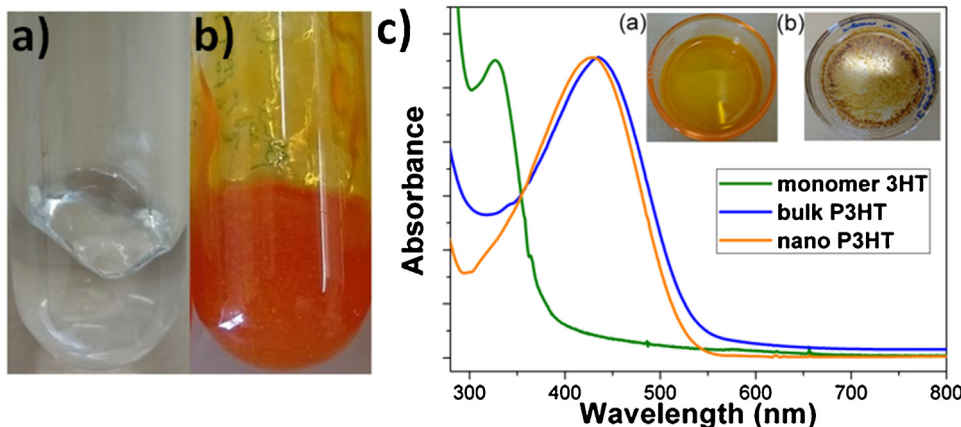


**Fig. 1.** Pictures of hexagonal mesophases doped with (a) 3HT monomer and (b) P3HT polymer; (c) Normalized UV-vis spectra of the 3HT monomer, nano P3HT, and bulk P3HT in chloroform. Inset: Pictures of nano P3HT extracted in ethanol (a) and after drying (b).

tor that has been mainly used for the fabrication of transistors, photovoltaic cells, strain sensors, and light emitting devices. P3HT appears to be the most commonly used CP in organic photovoltaics because of its desirable electronic properties [21]. The incorporation of P3HT into other semiconductors such as  $\text{TiO}_2$  or  $\text{Bi}_2\text{MoO}_6$  leads to the improvement of the photocatalytic activity [22,23].

Recently, we have shown that conjugated polymers (in particular Polydiphenylbutadiyne) (PDPB) and Poly(3,4-ethylenedioxythiophene) (PEDOT)) emerge as a new class of photocatalysts very active under visible light [24,25]. Oil-swollen surfactant stabilized hexagonal mesophases have been used as a versatile template to synthesize several metal and polymer nanomaterials, either in the aqueous phase or in the oil phase [26–33]. In this context, we have shown that the nanostructuration of PDPB and PEDOT polymers, thanks to their synthesis in a soft template formed by hexagonal mesophases, leads to an enhancement of their photocatalytic activity. [24,25]

Here, we show for the first time that nanostructures of P3HT are also highly efficient for the degradation of pollutants under UV and visible light. These photocatalysts, which are very stable with cycling, can furthermore be easily deposited on a flat solid support (quartz or glass) for photocatalytic application. Interestingly, we measure a much faster kinetics for the degradation of pollutant once P3HT nanostructures are deposited on a solid surface.

## 2. Experimental section

### 2.1. Materials

3-hexylthiophene (3HT) as monomer, iron (III) chloride as oxidative agent, cetyltrimethylammonium bromide (CTAB) ( $\geq 98\%$ ) as surfactant, sodium chloride (NaCl), toluene ( $> 99\%$ ), *n*-pentanol ( $\geq 99\%$ ) and phenol ( $\text{C}_6\text{H}_5\text{OH}$ ) were purchased from Sigma-Aldrich. Rhodamine B (RB) was purchased from Fluka. Titania (P25, surface area =  $50 \text{ m}^2 \text{ g}^{-1}$ , 80% Anatase, 20% Rutile and a small amount of amorphous  $\text{TiO}_2$ ) was obtained from Evonik for comparative photodegradation. All compounds were used as received. Ultra-pure water (Millipore System,  $18.2 \text{ M}\Omega \text{ cm}$ ) and ethanol ( $\geq 99\%$  for HPLC, purchased from Sigma-Aldrich) were used as solvents. All experiments were performed at room temperature.

### 2.2. Photocatalysts preparation

Poly(3-hexylthiophene) (P3HT) nanostructures (hereafter called nano P3HT) were synthesized inside the oil phase of hexagonal mesophases. The hexagonal mesophases were pre-

pared following the previously published method with some modifications. This system consists of surfactant and co-surfactant-stabilized oil (toluene) tubes regularly arranged on a triangular lattice in water. To prepare the hexagonal mesophases, 1.03 g of CTAB was first dissolved in 2 mL of sodium chloride 0.1 M and then, vortexed for a few minutes. The mixture was then let in an oven at 50 °C for 1 h to form a transparent and viscous micellar solution. Then, 1 mL of toluene containing 54  $\mu\text{L}$  of the 3HT monomer was added to the micellar solution under vortex. Subsequently, 2 mL of toluene containing 96 mg of  $\text{FeCl}_3$  was added, and the mixture was vortexed for a few minutes. This lead to an opaque unstable emulsion. The cosurfactant (20  $\mu\text{L}$  of *n*-pentanol) was added dropwise and strongly vortexed until an orange, translucent and birefringent gel (a hexagonal mesophase) was formed. The polymerization of 3-hexylthiophene was induced by oxidation with  $\text{FeCl}_3$ . To avoid the bulk polymerization, the monomer and oxidizing agent were never put together, but instead were dissolved in toluene separately and then added to the mixture during mesophase formation.

Bulk P3HT was synthesized in toluene without any surfactant. The ratio between monomer and oxidizing agent ( $\text{FeCl}_3$ ) was the same as that used for the synthesis of nano P3HT in mesophases.

After polymerization, the materials were extracted by adding ethanol and water, followed by centrifugation and washed several times to remove the excess of surfactant and oxidant. The polymer was then extracted with ethanol and dried for one night at 40 °C.

The photocatalytic activity of nano and bulk P3HT was compared to that of plasmonic titania and PDPB nanowires. Plasmonic titania ( $\text{TiO}_2$  modified with Ag nanoparticles) consist in small silver nanoparticles synthesized on  $\text{TiO}_2$  (P25) by radiolysis. The synthesis is described in details in reference 6. PDPB nanowires were synthesized using swollen hexagonal mesophases as soft template following the previously published method [24].

### 2.3. Material characterization

The mesophases before and after polymerization were analyzed using Small Angle X-Ray Scattering (SAXS). The mesophases were inserted in a glass capillaries of 1.5 mm diameter and high brightness low power X-Ray tube, coupled with an aspheric multilayer optic (GeniX 3D from Xenocs) was employed, which delivered an ultralow divergent beam (0.5 mrad). Scatterless slits were used to give a clean 0.87 mm diameter X-Ray spot with an estimated flux around  $35 \text{ mphs}^{-1}$  at the sample position. A transmission configuration was used. The scattered intensity was collected on a two dimensional Schneider 2D image plate detector prototype, at

a distance of 1.9 m from the sample. The experimental data were corrected for the background scattering and the sample transmission.

UV-vis absorption spectra of the monomer, bulk P3HT and nano P3HT were recorded in chloroform using a HP8543 spectrophotometer. Luminescence measurements were performed with a SpexFluorolog 1681 spectrofluorimeter equipped with a Hamamatsu R928 photomultiplier cooled down to  $-20^{\circ}\text{C}$ . The emission and excitation spectra were recorded at room temperature in the right angle configuration and not corrected by the detection system response. The maximum absorbance of the sample contained in a 1 cm quartz cuvette was below 0.1.

Maldi-TOF (Matrix Assisted Laser Desorption/Ionization Time of Flight) mass spectrometry was used to measure the degree of polymerization. The solution of P3HT in tetrahydrofuran (THF) was mixed with a matrix solution. The matrix-sample solution was then placed on a stainless steel plate. The spectra were obtained in the reflection mode and in the positive ion mode.

Attenuated Total reflectance (ATR-FTIR) spectroscopy was used for chemical identification of P3HT. ATR-FTIR spectra of pure 3HT monomer, bulk P3HT, or nano P3HT were recorded using a Bruker Vertex 70 FTIR spectrometer with diamond ATR attachment (PIKEMIRACLE crystal plated diamond/ZnSe) and a mercury-cadmium-telluride (MCT) detector with a liquid nitrogen cooling system. Scanning wavelength were varied from 4000 to 600  $\text{cm}^{-1}$  with a  $4\text{ cm}^{-1}$  spectral resolution using 100 repetition scans on average for each spectrum.

The morphology of nano P3HT and bulk P3HT, eventually combined with the chemical structure information, was determined by combining the classical atomic force microscope (AFM) with tunable pulsed laser as an Infrared (IR) source (AFMIR). We used a commercial setup, nanoIR (Anasys Instrument corp.) allowing us to cover the range from  $3600\text{ cm}^{-1}$  to  $1000\text{ cm}^{-1}$ . Drops of ethanolic solution of P3HT were directly deposited on the upper surface of ZnSe prism and dried at room temperature. The ZnSe prism is transparent in the mid-infrared and the tip of the AFM remains in contact with the sample. When the sample absorbs the IR laser pulse, it warms via the photothermal effect, resulting in a rapid thermal expansion of the absorbing region of the sample. The thermal expansion pulse impacts the tip of AFM cantilever and causes it to oscillate. As the amplitude of oscillations is proportional to the absorption, we are able to record infrared absorption spectra at a given point and to make chemical maps by scanning the surface at a given wavelength.

The polymer structures were also characterized using Transmission Electron Microscopy (TEM) JEOL JEM 100CX at an accelerating voltage of 100 kV. Few drops of sample (dispersed in ethanol) were deposited on carbon coated copper grids and dried under  $\text{N}_2$  flow. The images were collected using a CCD camera. Scanning Electron Microscope (SEM) images were acquired using a ZEISS Supra 55VP FEG-SEM at 1 kV with no conductive coating on top of the sample. The sample was prepared by depositing solution of nano P3HT in chloroform on quartz support and dried under  $\text{N}_2$  flow.

#### 2.4. Electrochemical analysis

The electrochemical setup was a three-electrodes cell, with a glassy carbon (GC) disk (2 mm diameter) drop-coated by P3HT film as the working electrode, a Pt wire as counter electrode, and a silver wire pseudo-reference electrode. This latter is calibrated as recommended by IUPAC [34] probing ferrocenium/ferrocene ( $\text{Fc}^+/\text{Fc}$ ) redox potential measured at the end of each experiment. Polymer samples (at a concentration of  $1\text{ mg mL}^{-1}$  in chloroform) were drop-casted onto the GC-electrode and then dried. The GC-electrode was immersed into the electrochemical cell containing acetonitrile with  $0.1\text{ M}$  tetrabutylammonium hexafluorophosphate (TBAPF<sub>6</sub>).

The compounds were electrochemically reduced prior to being oxidized between  $-2.1\text{ V}$  and  $+1.4\text{ V}$  at a scan rate of  $20\text{ mV/s}$ .

#### 2.5. Photocatalytic test

Phenol was chosen as model pollutant: it is a real pollutant, stable under irradiation (no photolysis), and its intermediate degradation products are well known. The photocatalytic activity of P3HT was evaluated for decomposition of phenol ( $\text{C}_6\text{H}_5\text{OH}$ ) in a quartz cell reactor with a 10 mm optical path containing  $3.5\text{ mL}$  of  $3.7 \times 10^{-3}\text{ mol L}^{-1}$  of phenol in the presence of  $1\text{ g L}^{-1}$  of P3HT. Other photocatalytic tests were also conducted with RB (as another model pollutant) at a concentration of  $4 \times 10^{-5}\text{ M}$  in the same irradiation conditions.

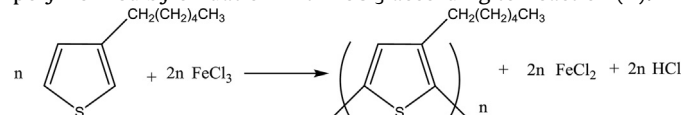
Before any photocatalytic tests, dark adsorption tests of bulk and nano P3HT were carried out, by putting the polymer samples into contact with the model pollutants in the absence of irradiation: The suspension containing P3HT in phenol solution was stirred for 3 h to ensure the homogeneity of the suspension. After 3 h contact, no adsorption of phenol and RB on the polymer nanostructures or on bulk P3HT could be detected.

The sample were irradiated under stirring with an Oriel 300 W Xenon lamp through an infrared water filter and an ultraviolet cut off filter (longpass filter GG400,  $\lambda \geq 400\text{ nm}$ ) for the experiment under visible light.

For photocatalytic test of P3HT on a solid support, 3 mg of P3HT was dissolved in chloroform and gently deposited on a quartz glass, then dried at room temperature. A P3HT –coated quartz glass was inserted into a 1 cm cell containing 3 mL of an aqueous solution with  $3.7 \times 10^{-3}\text{ mol L}^{-1}$  of phenol.  $400\text{ }\mu\text{L}$  of the solution was taken at different time intervals from the reactor and centrifuged before further analysis. HPLC (high performance liquid chromatography) was used to determine phenol concentration and to study its degradation while the RB concentration was determined by spectrophotometric method (at 550 nm). The Total Organic Carbon (TOC) was measured with a Shimadzu TOC-LCSH by IR after complete oxidation by catalytic combustion at  $680^{\circ}\text{C}$  on exclusive platinum catalyst, the inorganic carbon being removed by a previous acidification and air purging.

### 3. Results and discussion

Swollen hexagonal mesophases are used as templates for the synthesis of P3HT nanostructures. These mesophases are composed of oil-swollen surfactant tubes arranged on a triangular lattice in water. The hydrophobic domain of the mesophases can accommodate high concentrations (up to  $0.1\text{ M}$ ) of 3HT monomer, which is polymerized by oxidation with  $\text{FeCl}_3$  according to Reaction (1):



Here, polymerization proceeds inside the confined oil tubes (toluene phase) of diameter  $\approx 27\text{ nm}$ . Hexagonal mesophases containing only monomers are colorless (Fig. 1a), transparent and birefringent, while the mesophases containing  $\text{FeCl}_3$  are also translucent and birefringent, but yellow, because of the absorption properties of  $\text{FeCl}_3$ . The oxidant ( $\text{FeCl}_3$ ) and monomer (3HT) are dispersed in separate volumes of toluene, in order to avoid polymerization prior to mesophase formation. The hexagonal mesophases are characterized by small angle X-ray scattering (SAXS) (see Fig. S1 and Table S1 in Supplementary information). Once incorporated sequentially in the mesophase, the color of the mixture turns first into green-brown, and then orange upon continuous vortex (Fig. 1b). The as-prepared P3HT structures can be easily

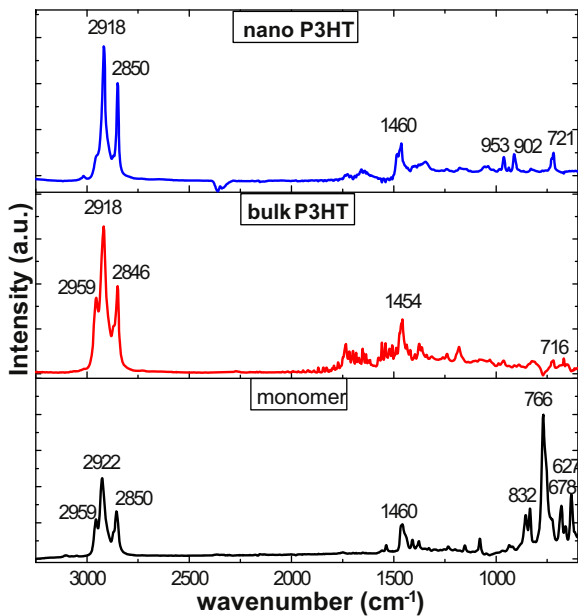


**Fig. 2.** ATR-FTIR spectra of the 3HT monomers and of nano P3HT and bulk P3HT polymers.

extracted from the mesophases by simple washing with ethanol, followed by centrifugation (insert a of Fig. 1c). After drying an orange solid powder of P3HT is obtained (Inset b of Fig. 1c).

Fig. 1c shows the UV-vis absorption spectra of the 3HT monomers and that of P3HT polymer structures (synthesized with and without mesophases, denoted respectively as nano P3HT and bulk P3HT). The 3HT monomer exhibits an absorption peak at 329 nm. After polymerization, the peak at 329 nm disappears, and a new peak around 428 nm for nano P3HT and 435 nm for bulk P3HT appears, which indicates the complete polymerization of P3HT. The absorption is due to the  $\pi-\pi^*$  interband transition. The optical band gap can be estimated from the absorption edge as equal to 550 nm (2.25 eV). The maximum molecular weight of nano P3HT, as determined by MalDI-TOF (Matrix Assisted Laser Desorption/Ionization Time of Flight) mass spectroscopy, is found to be 4668 g mol<sup>-1</sup> which corresponds to about 28 repeated units of 3HT monomers (See Fig. S2).

Fig. 2 shows attenuated total reflectance Fourier transform infrared spectroscopy (ATR-FTIR) spectra of the monomer 3HT, and of nano and bulk P3HT. The spectra of nano and bulk P3HT are similar, although their absorption bands are slightly shifted, and in good agreement with the literature [35]. Three peaks are observed in the interval (3000–2850) cm<sup>-1</sup> for all samples. These peaks are characteristic of C–H bonds on the hexyl side chain, and are assigned respectively to the asymmetric C–H stretching vibrations of  $-\text{CH}_3$  (2956 cm<sup>-1</sup>) and  $-\text{CH}_2-$  (2920 cm<sup>-1</sup>) moieties, as well as the symmetric C–H stretching vibration in  $-\text{CH}_2-$  (2850 cm<sup>-1</sup>) moieties. The peak around (1454–1460) cm<sup>-1</sup> (found also for all samples) is associated with a symmetric C=C ring stretching vibration. In the fingerprint region, the IR absorption peaks for 3HT monomer at 766 cm<sup>-1</sup> and 832 cm<sup>-1</sup> are ascribed to the C–H out-of-plane stretching vibration of the 2,5-substituted thiophene ring. These peaks are no longer observed for nano and bulk P3HT, which confirms the quantitative polymerization of the thiophene monomers. The peaks at 627 and 678 cm<sup>-1</sup> are associated to the absorption of C–S–C bonds of the thiophene ring. The characteristic in-plane and out-of-plane rocking vibration of  $-(\text{CH}_2)_n-$  group can also be observed at (716–720) cm<sup>-1</sup>.

Transmission Electron Microscopy (TEM) images (Fig. 3a–b) show that bulk P3HT forms large aggregates of several hundred

nanometers. By contrast, the polymer nanostructures synthesized in hexagonal mesophases are constituted of connected nanowires of diameter about 30 nm. Note that the diameter of the P3HT nanowires corresponds to the diameter of the cylinder of the hexagonal mesophase determined by SAXS (see Fig. S1 and Table S1) attesting the templating effect of the soft mould.

Atomic Force Microscopy combined with infrared spectroscopy (AFMIR) allows concomitant investigation of the surface topography and chemical structure. The surface topography of P3HT synthesized in hexagonal mesophases highlights the presence of elongated like structures while P3HT synthesized in bulk solution shows large plates (around 10  $\mu\text{m}$  size), which were probably formed by aggregation of smaller particles on the ZnSe substrate during deposition (Fig. 3c, d). Fig. S3 shows the nanoIR spectrum of nano P3HT in the (1000–3200) cm<sup>-1</sup> region, which is quite similar to that measured using ATR-FTIR. Chemical mapping at characteristic wavenumbers for the polymer, 1456 cm<sup>-1</sup> (associated to the symmetric C=C ring stretching vibration from thiophene ring) and 2928 cm<sup>-1</sup> (due to the vibration of  $-\text{CH}_2-$  from hexyl side chain) confirms that the topography obtained by AFM is actually that of the polymer (Fig. 3e–h).

#### 4. Photocatalytic tests

The photocatalytic activity of P3HT is evaluated for water depollution. Phenol is chosen as a model pollutant, as it has long been proposed as standard test molecule [36]. Prior to any photocatalytic tests, dark adsorption tests of bulk P3HT and nano P3HT are performed, by putting into contact the polymer samples with the model pollutants in the absence of irradiation. In this case, no adsorption is observed on the polymer structures. The photocatalytic activity of bulk and nano P3HT was evaluated by measuring the decomposition rate of phenol in water under both UV-vis (xenon lamp) and visible light (using a long pass filter  $\lambda > 400$  nm) (Fig. 4). The photocatalytic activities of bulk P3HT and nano P3HT are compared to that of commercial TiO<sub>2</sub>, P25 (which is very active under UV light) and to that of nanofibers of PDPB, which have been reported recently [24]. Nano P3HT demonstrates a good photocatalytic activity for phenol degradation under UV-vis light: a 25% degradation is reached after 15 min, while with bulk P3HT 13%, degradation is achieved after the same irradiation time (Fig. 4a). This activity is higher than that of PDPB nanofibers under UV light (but much less efficient than that of P25) (see Figs. S4, S5 and Table S2). The total mineralization of phenol is followed using as a common technique, the disappearance of the total organic carbon (TOC) for expressing the detoxification level of water. The P3HT nanostructures were able to fully oxidize the organic pollutant, with an almost complete mineralization of carbon into CO<sub>2</sub> and H<sub>2</sub>O. Indeed, TOC measurements indicate about 87% of mineralization of phenol after 240 min under UV light. These results suggest that the conducting polymer nanostructures are able to mineralize organic pollutants.

Interestingly, under visible light, nano P3HT still exhibits a high photocatalytic activity, higher than that of bulk P3HT: 16% photodegradation of phenol is achieved after a 240 min irradiation with nano P3HT, while only 3% degradation is obtained with bulk P3HT (Fig. 4b). Nevertheless, this activity is lower than that of Ag-TiO<sub>2</sub> and PDPB under visible light (see Figs. S6, S7 and Table S3). Other photocatalytic tests conducted with Rhodamine B also show high photocatalytic activity of the P3HT nanostructures under UV and visible light (see Fig. S8).

For applications, it is important to obtain stable photocatalysts. Therefore, the stability of P3HT nanostructures with cycling is investigated (Fig. 4c). We find that the photocatalytic activity

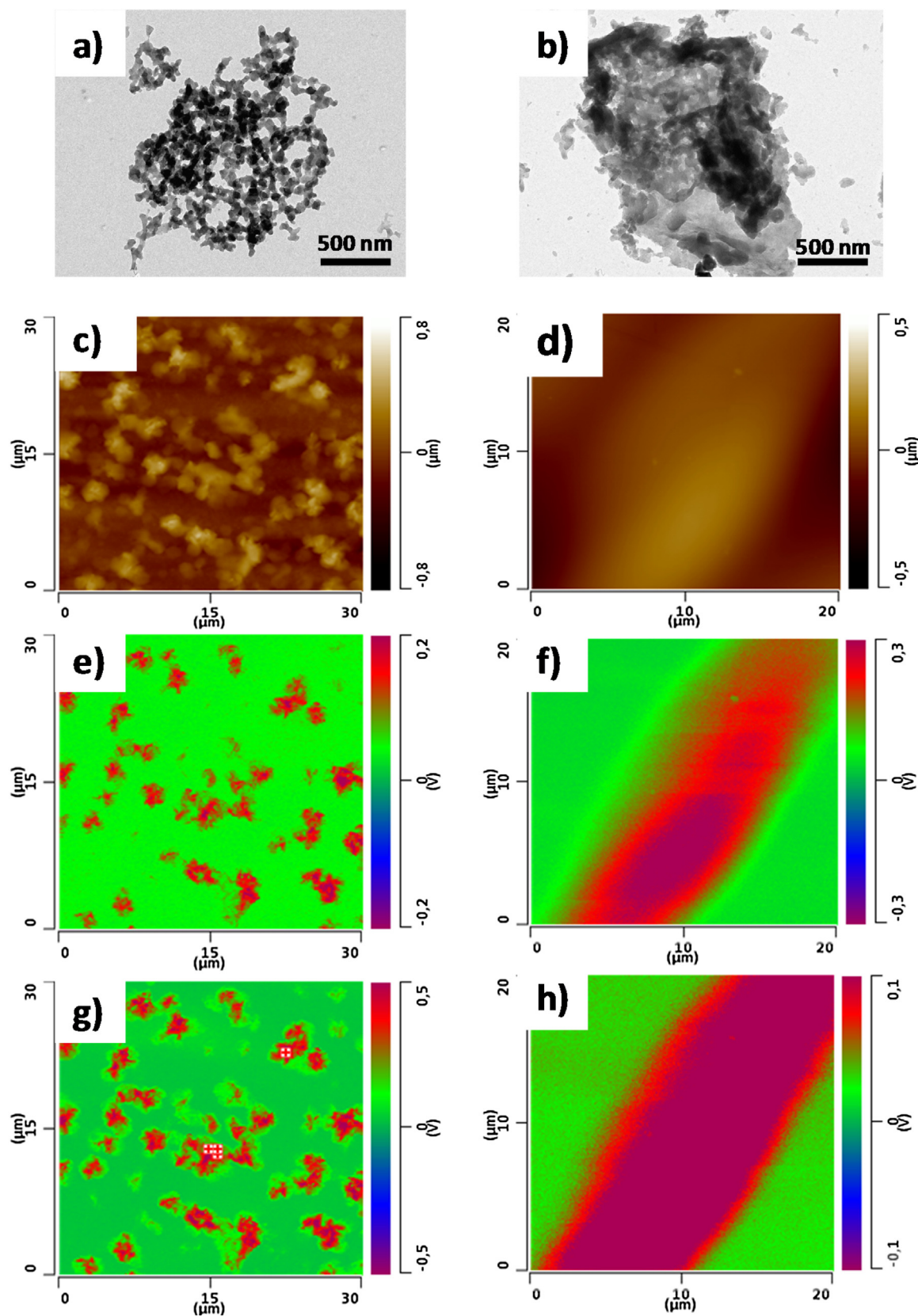


**Fig. 3.** TEM images for nano P3HT (a) and bulk P3HT (b), AFM topography for nano P3HT (c) and bulk P3HT (d), Chemical mapping at  $1456\text{ cm}^{-1}$  for nano (e) and bulk (f) P3HT, Chemical mapping at  $2928\text{ cm}^{-1}$  for nano (g) and bulk (h) P3HT.

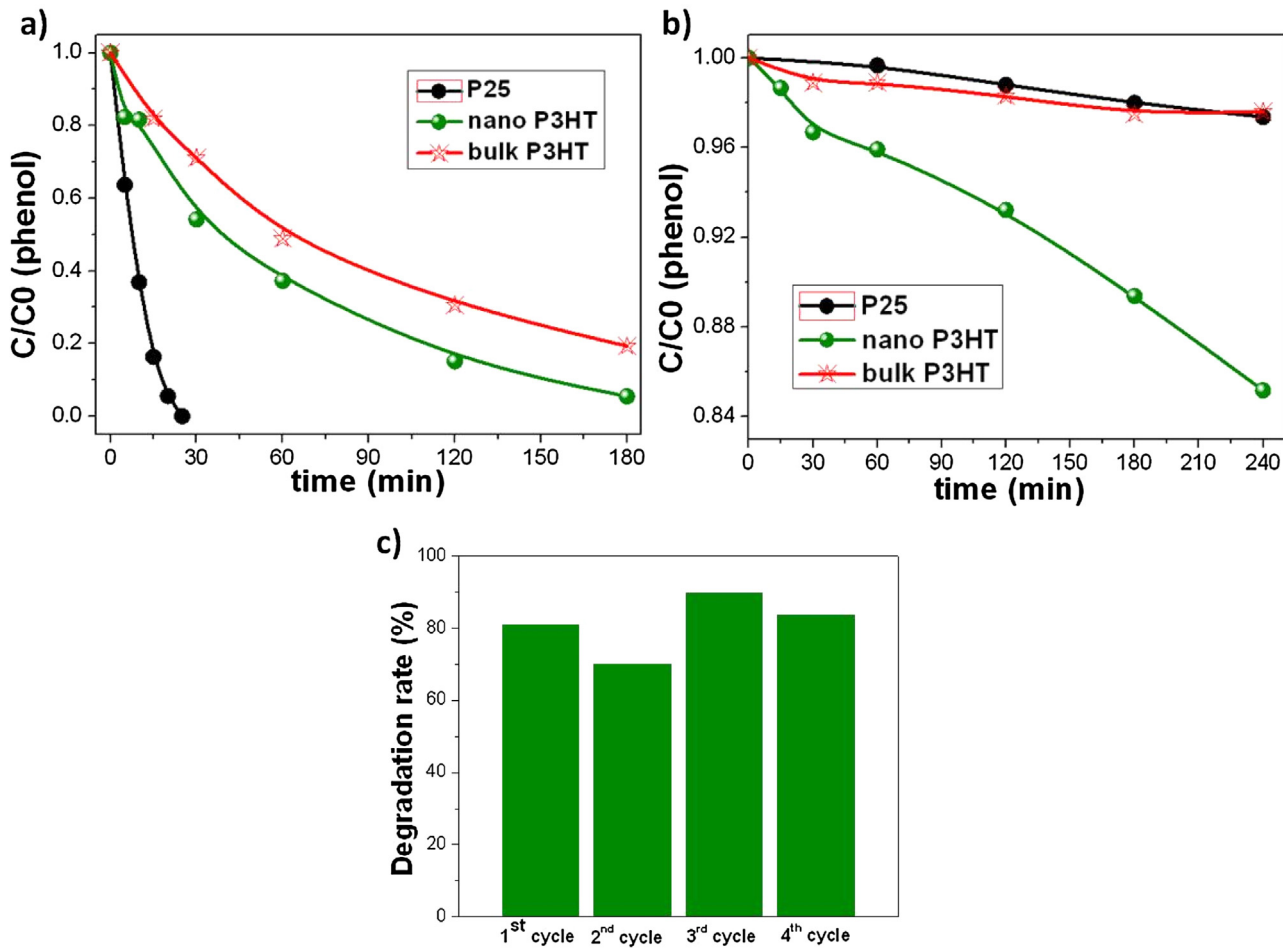


**Fig. 4.** Photocatalytic tests of P3HT (in suspension) under UV-vis (a) and visible light ( $\lambda > 400$  nm) (b) for the degradation of phenol in water solution; (c) Photocatalytic degradation rate of phenol using nano P3HT up to 4 cycles after 180 min irradiation under UV-vis light irradiation.

is very stable up to 4 cycles, suggesting that P3HT nanostructures could be efficiently reused after repeated cycles.

The difference in the photocatalytic activity between nano and bulk conjugated polymer nanostructures have already been reported for other conjugated polymers (PDPB and PEDOT) and have been assigned to the presence of more defects in bulk polymers favoring higher electron-hole recombination [24,25].

In order to understand the origin of the photocatalytic activity of P3HT nanostructures under UV and visible light, it is necessary to investigate their electronic properties. The oxidation and reduction potentials of bulk and nano P3HT are determined under similar experimental conditions to estimate, using cyclic voltammetry (CV) measurements, both the energy level of the highest occupied molecular orbital (HOMO) and the energy of lowest unoccupied molecular orbital (LUMO) from the ionization potential and the electronic affinity, respectively, as well as the band gap. We find that the main *p*-doping (oxidation) process occurs at onset potentials of +0.79 V (bulk P3HT) and +0.81 V (nano P3HT) while *n*-doping starts at -1.82 V (bulk P3HT) and -1.76 V (nano P3HT) yielding an electrochemical gap  $E_{\text{gap,elec}}$ . 2.61 eV (bulk P3HT) and 2.57 eV (nano P3HT) in a first approximation as shown in Fig. 5. Further, a careful look at CV may give hints to explain the differences between the photocatalytic properties of nano P3HT and bulk P3HT, especially in the *p*-doping part. Indeed, a very small current can be recorded between -0.1 V to 0.5 V with an onset at around 0.095 V vs. Ag before the main onset oxidation for nano P3HT. Upon *p*-dedoping process, a reverse behavior (small negative current) is also observed

in the same potential window. This effective redox system (see arrow in Fig. 5a) is typical of the presence of structural defects hence creating interband/microstates energetic levels. As a matter of fact, at the vicinity of these defects, the bandgap is much lower and the HOMO level is raised (see Fig. 5). The low bandgap implies the possibility of a more efficient injection of carriers, potentially useful for applications in optoelectronics or electrocatalysis. Such interband levels have already been observed in the case of PDPB [24].

## 5. Photocatalytic mechanism

Light irradiation of P3HT with photons of energy exceeding (or equal to) the band gap ( $E \geq 2.6$  eV or  $\lambda \leq 477$  nm) induces the formation of excitons and charge carriers. Their relaxation generates luminescence. The absorption and emission properties of P3HT as well as the dynamics of the excited states and charges have already been studied, both in solution and in films, mainly for regioregular P3HT [37–41]. We find that nano P3HT presents fluorescent properties, but the emission spectrum depends on the excitation wavelength (Fig. 6a). For excitation above 400 nm the dependence is weak as the emission spectrum exhibits a similar broad structureless band with a maximum slightly shifted, from 563 ( $\lambda_{\text{exc}} = 400$  nm) to 561 nm ( $\lambda_{\text{exc}} = 450$  nm). By contrast, for excitation below 400 nm, the emission spectrum changes more drastically as a shoulder appears around 480 nm, which suggests the presence of another emissive state. That is confirmed by the excitation spectra registered at different wavelengths (Fig. 6b).

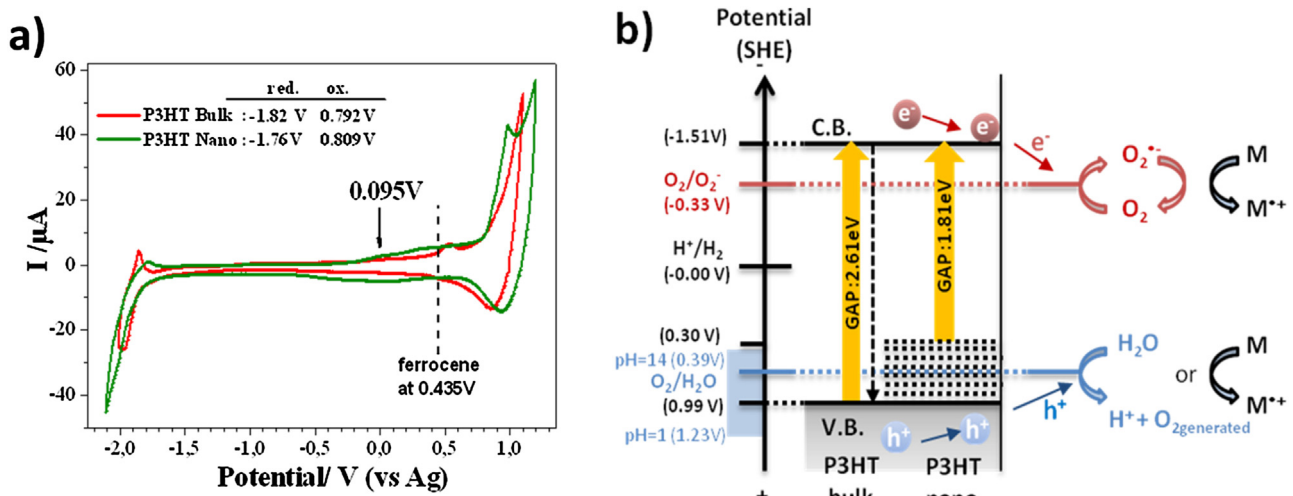


**Fig. 5.** (a) Cyclic voltammometry of bulk (red curve) and nano P3HT (green curve) recorded at 20 mV/s in acetonitrile and 0.1 M TBAPF<sub>6</sub>. Ferrocenium/ferrocene (Fc<sup>+</sup>/Fc) redox potential has been measured at the end of each experiment in order to calibrate the pseudo reference electrode (0.435 V vs. Ag in the present study). The HOMO/LUMO energetic levels of P3HT are determined as follows: E<sub>HOMO</sub> (eV) from ionization potential = -4.8-e (E<sub>ox.onset</sub>-0.435) and E<sub>LUMO</sub> (eV) from electronic affinity = -4.8-e (E<sub>red.onset</sub>-0.435). (b) Possible photocatalytic mechanism with charge separation in nano and bulk P3HT with both electron reducing oxygen and hole oxidizing water. Consequently, the holes and generated oxidative radicals can oxidize organic pollutants (noted as M). O<sub>2</sub> generated at the valence band level (V.B.) can contribute to the O<sub>2</sub> reduction at the conduction band level (C.B.). (For interpretation of the references to colour in this figure legend, the reader is referred to the web version of this article.)

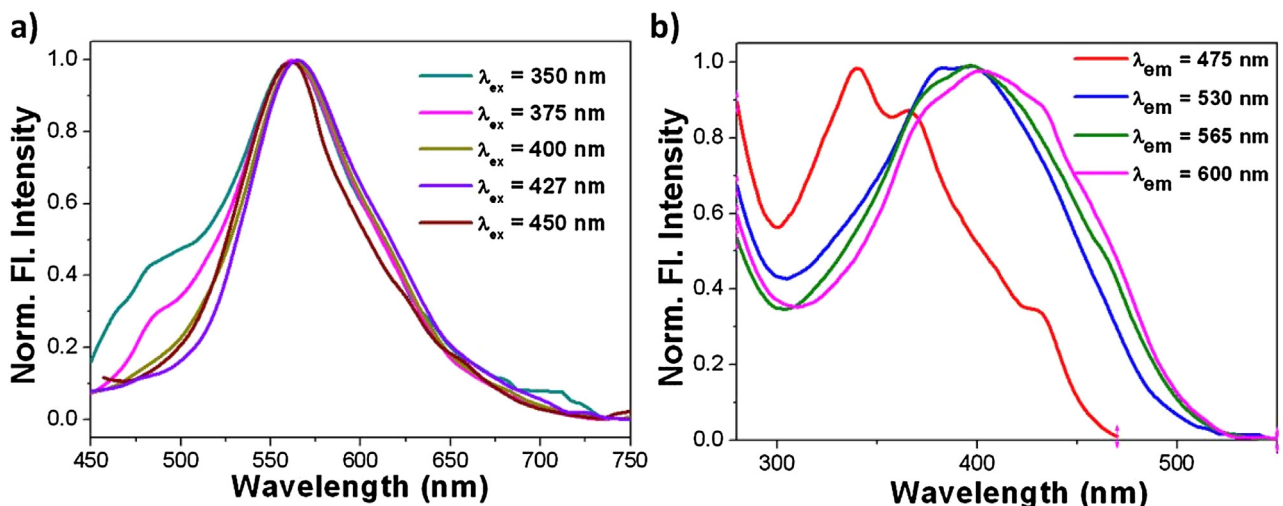


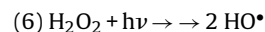
**Fig. 6.** Normalized emission (a) and excitation (b) spectra of nano P3HT in chloroform.

Indeed, the excitation spectra obtained for the main emission band peaking around 560 nm are alike presenting a broad band with a maximum around 400 nm and resemble the absorption spectrum. In contrast, the excitation spectrum related to the emission at 475 nm differs significantly: it is structured with a maximum at ~340 nm and two features at ~370 and ~430 nm, revealing the existence of higher energy excited states that do not relax entirely to the lowest emissive states. Consequently, excitation in the UV domain (below 380 nm) does not generate the same excited states as the excitation in the visible part, which may account for different photocatalytic activities under UV and visible light. A detailed study of the excited states and charge carriers is under progress.

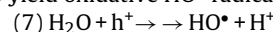
When electrons and holes escape from recombination, they can migrate to the surface and react with oxygen, water or other molecules at the interface. Electrons react with oxygen to form the oxidizing O<sub>2</sub><sup>•-</sup> superoxide radical (E<sup>0</sup> (O<sub>2</sub>/O<sub>2</sub><sup>•-</sup>) = -0.33 V<sub>SHE</sub>):



However, O<sub>2</sub><sup>•-</sup> is very reactive and can oxidize molecules and transform into HO<sup>•</sup> through the following reactions:



While in HOMO level, the holes might react with HO<sup>•</sup> (or H<sub>2</sub>O) to yield oxidative HO<sup>•</sup> radicals:



In order to identify the species that are responsible for photodegradation activity of nano P3HT, experiments were carried out with Cu<sup>2+</sup> and 2-propanol as electrons and holes scavengers, respectively. Data show that the presence of Cu<sup>2+</sup> slows down the degradation kinetics (Fig. S8). Cu<sup>2+</sup> reacts with electrons to yield Cu<sup>+</sup>, and this reaction is in competition with reaction (2). The presence of Cu<sup>2+</sup> causes a decrease in the production of O<sub>2</sub><sup>•-</sup> in the photocatalytic system, which leads to a decrease in the degrada-

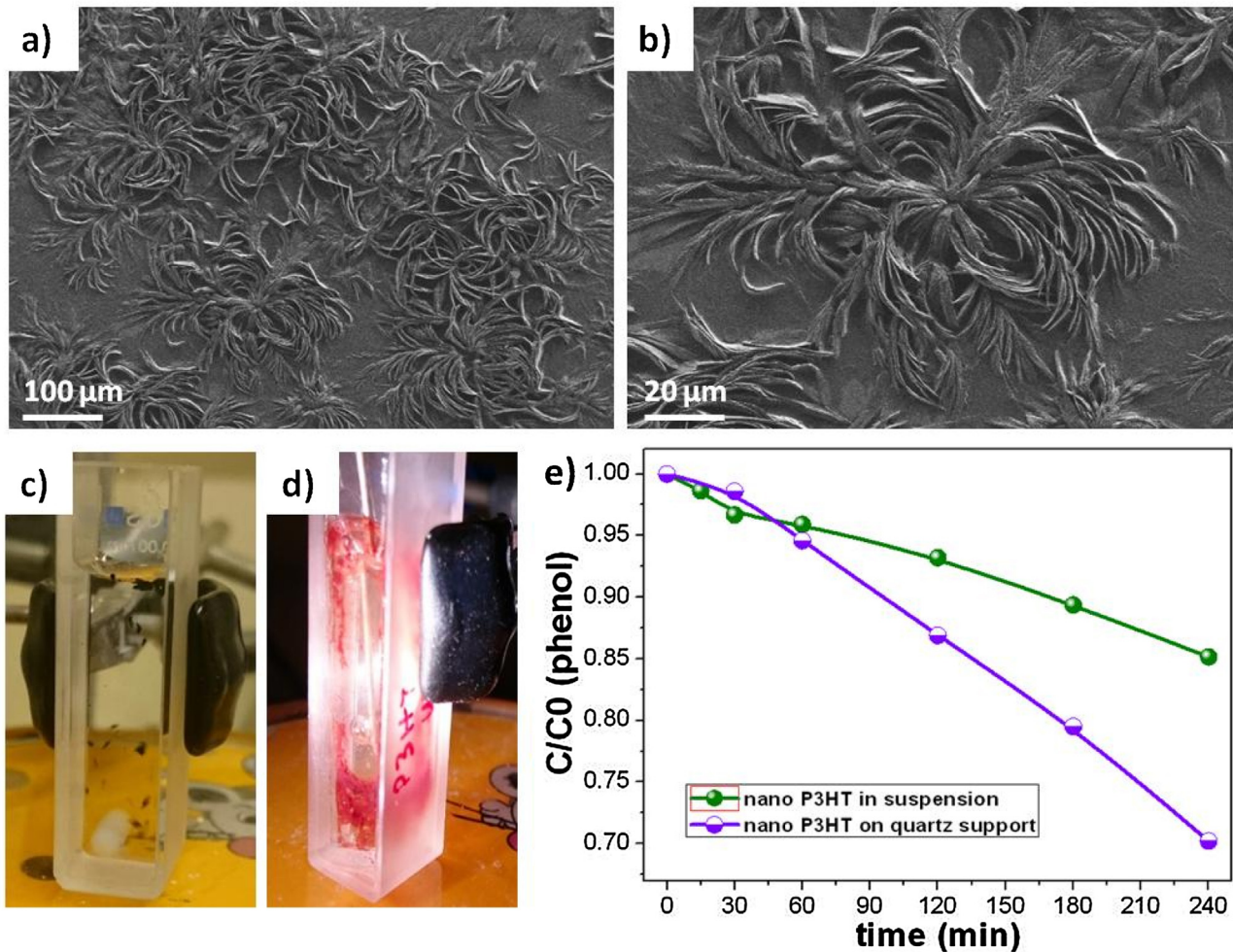


**Fig. 7.** (a–b) SEM images of nano P3HT deposited on a quartz slide (from a chloroform solution) at two different magnifications; (c) nano P3HT suspension in aqueous solution containing phenol; (d) A quartz slide coated with nano P3HT inside a quartz cell containing a phenol solution irradiated with visible light; (e) Photocatalytic degradation of phenol using nano P3HT in suspension and nano P3HT on a quartz slide under visible light.

tion kinetics. The photodegradation efficiency of phenol is reduced from 94% to 40% in the presence of 0.01 M of Cu<sup>2+</sup> after 3 h under UV-vis light irradiation (see Fig. S9). In addition, in the absence of O<sub>2</sub>, the activity of P3HT for phenol degradation decreases from 95% to 30% after 3 h UV-vis irradiation (Fig. S10). Furthermore, experiments have been conducted in the presence of 2-propanol known to scavenge the holes and HO• radicals very efficiently. The experiments conducted in the presence of O<sub>2</sub> and 2-propanol do not show any decrease in photocatalytic degradation of phenol (Fig. S11). According to the HOMO level of P3HT, the reaction between the holes and H<sub>2</sub>O is not thermodynamically favorable. Additional experiments are conducted with other scavengers: Benzoquinone and *tert*-butanol are used as O<sub>2</sub>•<sup>−</sup> (superoxide radical) and HO• scavengers, respectively. Fig. S12 shows that the presence of *tert*-butanol as HO• radical scavenger does not inhibit the photocatalytic activity of P3HT for phenol degradation, while the photocatalytic tests conducted with benzoquinone show no degradation of phenol. All these experiments prove that photodegradation of phenol by P3HT is mainly caused by O<sub>2</sub>•<sup>−</sup> superoxide radical formed from the reduction of oxygen (O<sub>2</sub>) or generated oxygen (O<sub>2</sub> generated).

Moreover, a remarkable result is that phenol degradation is faster with nano P3HT than with bulk P3HT (Fig. 4a and b). Several phenomena could explain those results. First, the nanometric size is expected to induce an increase of the specific surface area, which involves degradation reactions. Second, higher electron-hole

recombination is expected to occur in bulk P3HT because of higher volume and higher number of defects. Finally, the presence of microstates above the HOMO level for nano P3HT, as observed in CV measurements, is certainly crucial. Indeed, under illumination, the holes can react more easily with water to form oxygen with microstate energy levels close to E<sup>0</sup>(H<sub>2</sub>O/O<sub>2</sub>).

A possible mechanism for the oxidation of organic pollutants is proposed based on the band gap structure of P3HT and on the experiments with scavengers. Fig. 5b summarizes the charge carrier generation under irradiation and formation of ROS (Reactive Oxygen Species) (HO• and O<sub>2</sub>•<sup>−</sup>) responsible for the oxidation and degradation of the pollutants. These results confirm that O<sub>2</sub>•<sup>−</sup> is the main involved radical in the photocatalytic mechanism with P3HT (Fig. 5b).

### 5.1. Deposition of nano P3HT on a support for photocatalytic application

Because of its chemical structure, P3HT is very hydrophobic. Hence, P3HT nanostructures aggregate in water, resulting in a loss of surface area. Therefore, the photocatalytic tests in water suspensions containing phenol are not optimized, and explain the high uncertainties (10%) obtained with degradation tests (see for example Fig. 4c). On the other hand, for practical applications, it is important to avoid the separation step of the powder in suspension

and to develop deposition of the photocatalytic material on solid supports such as quartz slides, glass, fabric fibers, etc. Fig. 7a and b show Scanning Electron Microscopy (SEM) images of the P3HT nanostructures on quartz slides. When deposited on a flat support, the nanostructures self-assemble upon chloroform (used as solvent) evaporation because of London interactions between the non-polar carbon chains and  $\pi$ - $\pi$  stacking between the polarizable aromatic rings to form large plates forming flowers. Fig. 7c shows a suspension of P3HT nanostructures in a quartz cell containing an aqueous solution with phenol and Fig. 7d shows a quartz slide coated with nano P3HT inside a quartz cell containing a phenol solution irradiated with visible light. Photocatalytic tests are performed with P3HT deposited on quartz slides from a suspension in chloroform. Fig. 7e shows that phenol degradation kinetics is highly accelerated with deposited P3HT nanostructures (see also Fig. S13 and Table S4). This is the first time that conjugated polymer nanostructures are deposited on a support for photocatalytic applications. This result shows that the photocatalytic activity can be much enhanced with the supported conjugated polymers photocatalysts (contrary to what it is generally obtained with deposited  $TiO_2$ ) [8] and opens new perspectives for applications because no separation step is required. Optimization of the deposition of the CP on different supports is under study.

## 6. Conclusion

In conclusion, P3HT nanostructures synthesized in hexagonal mesophases present a high photocatalytic activity under UV and visible light. These photocatalysts are very stable with cycling. Our results demonstrate that  $O_2^{\bullet-}$  is the main radical responsible for the degradation of phenol taken as model pollutant. These conjugated polymer nanostructures can be easily deposited on solid supports. When deposited on quartz slides, the photocatalytic activity of the polymer nanostructures is much enhanced. These results open new perspectives for application of these conjugated polymers in photocatalytic reactors and in self-cleaning surfaces. Further studies will optimize the deposition of these nanostructures on different supports for practical applications.

## Appendix A. Supplementary data

Supplementary data associated with this article can be found, in the online version, at <http://dx.doi.org/10.1016/j.apcatb.2017.02.069>.

## References

- [1] P.V. Kamat,  $TiO_2$  nanostructures: recent physical chemistry advances, *J. Phys. Chem. C* 116 (2012) 11849–11851, <http://dx.doi.org/10.1021/jp305026h>.
- [2] M.G. Mendez Medrano, E.K. Kowalska, A. Lehoux, A. Herissan, B. Ohtani, S. Rau, C. Colbeau-Justin, J.L. Rodriguez Lopez, H. Remita, Surface modification of  $TiO_2$  with Au nanoclusters for efficient water treatment and hydrogen generation under visible light, *J. Phys. Chem. C* (2016), <http://dx.doi.org/10.1021/acs.jpcc.6b06854>.
- [3] Z. Bian, T. Tachikawa, P. Zhang, M. Fujitsuka, T. Majima, Au/ $TiO_2$  superstructure-Based plasmonic photocatalysts exhibiting efficient charge separation and unprecedented activity, *J. Am. Chem. Soc.* 136 (2014) 458–465, <http://dx.doi.org/10.1021/ja410994f>.
- [4] E. Kowalska, O.O.P. Mahaney, R. Abe, B. Ohtani, Visible-light-induced photocatalysis through surface plasmon excitation of gold on titania surfaces, *Phys. Chem. Chem. Phys.* 12 (2010) 2344–2355, <http://dx.doi.org/10.1039/B917399D>.
- [5] P.V. Kamat, Manipulation of charge transfer across semiconductor interface. a criterion that cannot be ignored in photocatalyst design, *J. Phys. Chem. Lett.* 3 (2012) 663–672, <http://dx.doi.org/10.1021/jz201629p>.
- [6] E. Grabowska, A. Zaleska, S. Sorgues, M. Kunst, A. Etcheberry, C. Colbeau-Justin, H. Remita, Modification of titanium(IV) dioxide with small silver nanoparticles: application in photocatalysis, *J. Phys. Chem. C* 117 (2013) 1955–1962, <http://dx.doi.org/10.1021/jp3112183>.
- [7] Q. Luo, L. Bao, D. Wang, X. Li, J. An, Preparation and strongly enhanced visible light photocatalytic activity of  $TiO_2$  nanoparticles modified by conjugated derivatives of polyisoprene, *J. Phys. Chem. C* 116 (2012) 25806–25815, <http://dx.doi.org/10.1021/jp308150j>.
- [8] S. Cassaignon, C. Colbeau-Justin, O. Durupthy, Titanium Dioxide in Photocatalysis, in: R. Brayner, F. Fiévet, T. Coradin (Eds.), Nanomater. Danger Promise Chem. Biol. Perspect., Springer London, London, 2013: pp. 153–188. 10.1007/978-1-4471-4213-3\_6.
- [9] S. Linic, P. Christopher, D.B. Ingram, Plasmonic-metal nanostructures for efficient conversion of solar to chemical energy, *Nat. Mater.* 10 (2011) 911–921, <http://dx.doi.org/10.1038/nmat3151>.
- [10] X. Wang, K. Maeda, A. Thomas, K. Takanabe, G. Xin, J.M. Carlsson, K. Domen, M. Antonietti, A metal-free polymeric photocatalyst for hydrogen production from water under visible light, *Nat. Mater.* 8 (2009) 76–80, <http://dx.doi.org/10.1038/nmat2317>.
- [11] N. Serpone, A.V. Emeline, Semiconductor photocatalysis – past, present, and future outlook, *J. Phys. Chem. Lett.* 3 (2012) 673–677, <http://dx.doi.org/10.1021/jz300071j>.
- [12] C. Su, R. Tandiana, B. Tian, A. Sengupta, W. Tang, J. Su, K.P. Loh, Visible-light photocatalysis of aerobic oxidation reactions using carbazolic conjugated microporous polymers, *ACS Catal.* 6 (2016) 3594–3599, <http://dx.doi.org/10.1021/acscatal.6b00443>.
- [13] J. Liu, Y. Liu, N. Liu, Y. Han, X. Zhang, H. Huang, Y. Lifshitz, S.-T. Lee, J. Zhong, Z. Kang, Metal-free efficient photocatalyst for stable visible water splitting via a two-electron pathway, *Science* 347 (2015) 970–974, <http://dx.doi.org/10.1126/science.aaa3145>.
- [14] Polyacetylene, (CH)x: n-type and p-type doping and compensation, *Appl. Phys. Lett.* 33 (1978) 18–20, <http://dx.doi.org/10.1063/1.90166>.
- [15] J.D. Yuen, R. Menon, N.E. Coates, E.B. Namdas, S. Cho, S.T. Hannahs, D. Moses, A.J. Heeger, Nonlinear transport in semiconducting polymers at high carrier densities, *Nat. Mater.* 8 (2009) 572–575, <http://dx.doi.org/10.1038/NMAT2470>.
- [16] I.B. Martini, I.M. Craig, W.C. Molenkamp, H. Miyata, S.H. Tolbert, B.J. Schwartz, Controlling optical gain in semiconducting polymers with nanoscale chain positioning and alignment, *Nat. Nanotechnol.* 2 (2007) 647–652, <http://dx.doi.org/10.1038/nano.2007.294>.
- [17] D. Ma, M. Aguiar, J.A. Freire, I.A. Hümmelgen, Organic reversible switching devices for memory applications, *Adv. Mater.* 12 (2000) 1063–1066, [http://dx.doi.org/10.1002/1521-4095\(200007\)12:14<1063::AID-ADMA1063>3.0.CO;2-9](http://dx.doi.org/10.1002/1521-4095(200007)12:14<1063::AID-ADMA1063>3.0.CO;2-9).
- [18] H. Sirringhaus, N. Tessler, R.H. Friend, Integrated optoelectronic devices based on conjugated polymers, *Science* 280 (1998) 1741–1744, <http://dx.doi.org/10.1126/science.280.5370.1741>.
- [19] Z. Yin, Q. Zheng, Controlled synthesis and energy applications of one-dimensional conducting polymer nanostructures: an overview, *Adv. Energy Mater.* 2 (2012) 179–218, <http://dx.doi.org/10.1002/aenm.201100560>.
- [20] S. Ghosh, T. Maiyalagan, R.N. Basu, Nanostructured conducting polymers for energy applications: towards a sustainable platform, *Nanoscale* 8 (2016) 6921–6947, <http://dx.doi.org/10.1039/C5NR08803H>.
- [21] S. Günes, H. Neugebauer, N.S. Sariciftci, Conjugated polymer-Based organic solar cells, *Chem. Rev.* 107 (2007) 1324–1338, <http://dx.doi.org/10.1021/cr050149z>.
- [22] D. Wang, J. Zhang, Q. Luo, X. Li, Y. Duan, J. An, Characterization and photocatalytic activity of poly(3-hexylthiophene)-modified  $TiO_2$  for degradation of methyl orange under visible light, *J. Hazard. Mater.* 169 (2009) 546–550, <http://dx.doi.org/10.1016/j.jhazmat.2009.03.135>.
- [23] T. Zheng, J. Xu, Z. Zhang, H. Zeng, P3HT/ $Bi_2MoO_6$  heterojunction with enhanced photocatalytic activity, *Mater. Lett.* 164 (2016) 640–643, <http://dx.doi.org/10.1016/j.matlet.2015.11.089>.
- [24] S. Ghosh, N.A. Kouamé, L. Ramos, S. Remita, A. Dazzi, A. Deniset-Besseau, P. Beaunier, F. Goubard, P.-H. Aubert, H. Remita, Conducting polymer nanostructures for photocatalysis under visible light, *Nat. Mater.* 14 (2015) 505–511, <http://dx.doi.org/10.1038/nmat4220>.
- [25] S. Ghosh, N.A. Kouame, S. Remita, L. Ramos, F. Goubard, P.-H. Aubert, A. Dazzi, A. Deniset-Besseau, H. Remita, Visible-light active conducting polymer nanostructures with superior photocatalytic activity, *Sci. Rep.* 5 (2015) 18002, <http://dx.doi.org/10.1038/srep18002>.
- [26] E. Pena dos Santos, M.S. Tokumoto, G. Surendran, H. Remita, C. Bourgaux, P. Dieudonné, E. Prouzet, L. Ramos, Existence and stability of new Nanoreactors: highly swollen hexagonal liquid crystals, *Langmuir* 21 (2005) 4362–4369, <http://dx.doi.org/10.1021/la047092g>.
- [27] G. Surendran, M.S. Tokumoto, E. Pena dos Santos, H. Remita, L. Ramos, P.J. Kooyman, C.V. Santilli, C. Bourgaux, P. Dieudonné, E. Prouzet, Highly swollen liquid crystals as new reactors for the synthesis of nanomaterials, *Chem. Mater.* 17 (2005) 1505–1514, <http://dx.doi.org/10.1021/cm0484495>.
- [28] G. Surendran, F. Ksar, L. Ramos, B. Keita, L. Nadjo, E. Prouzet, P. Beaunier, P. Dieudonné, F. Audonnet, H. Remita, Palladium nanoballs synthesized in hexagonal mesophases, *J. Phys. Chem. C* 112 (2008) 10740–10744, <http://dx.doi.org/10.1021/jp801703z>.
- [29] F. Ksar, G. Surendran, L. Ramos, B. Keita, L. Nadjo, E. Prouzet, P. Beaunier, A. Hagège, F. Audonnet, H. Remita, Palladium nanowires synthesized in hexagonal mesophases: application in ethanol electrooxidation, *Chem. Mater.* 21 (2009) 1612–1617, <http://dx.doi.org/10.1021/cm803492j>.
- [30] A. Lehoux, L. Ramos, P. Beaunier, D.B. Uribe, P. Dieudonné, F. Audonnet, A. Etcheberry, M. José-Yacamán, H. Remita, Tuning the porosity of bimetallic nanostructures by a soft templating approach, *Adv. Funct. Mater.* 22 (2012) 4900–4908, <http://dx.doi.org/10.1002/adfm.201200666>.

- [31] F. Ksar, L. Ramos, B. Keita, L. Nadjo, P. Beaunier, H. Remita, Bimetallic palladium-gold nanostructures: application in ethanol oxidation, *Chem. Mater.* 21 (2009) 3677–3683, <http://dx.doi.org/10.1021/cm901364w>.
- [32] S. Ghosh, H. Remita, L. Ramos, A. Dazzi, A. Deniset-Besseau, P. Beaunier, F. Gouvard, P.-H. Aubert, F. Brisset, S. Remita, PEDOT nanostructures synthesized in hexagonal mesophases, *New J. Chem.* 38 (2014) 1106, <http://dx.doi.org/10.1039/c3nj01349a>.
- [33] S. Ghosh, L. Ramos, S. Remita, A. Dazzi, A. Deniset-Besseau, P. Beaunier, F. Gouvard, P.-H. Aubert, H. Remita, Conducting polymer nanofibers with controlled diameters synthesized in hexagonal mesophases, *New J. Chem.* 39 (2015) 8311–8320, <http://dx.doi.org/10.1039/C5NJ00826C>.
- [34] G. Gritzner, J. Kuta, Recommendations on reporting electrode potentials in nonaqueous solvents (recommendations 1983), *Pure Appl. Chem.* 56 (1984), <http://dx.doi.org/10.1351/pac198456040461>.
- [35] X. Qiao, X. Wang, Z. Mo, The effects of different alkyl substitution on the structures and properties of poly(3-alkylthiophenes), *Synth. Met.* 118 (2001) 89–95, [http://dx.doi.org/10.1016/S0379-6779\(00\)00286-1](http://dx.doi.org/10.1016/S0379-6779(00)00286-1).
- [36] N. Serpone, G. Sauv , R. Koch, H. Tahiri, P. Pichat, P. Piccinini, E. Pelizzetti, H. Hidaka, Standardization protocol of process efficiencies and activation parameters in heterogeneous photocatalysis: relative photonic efficiencies  $\zeta_r$ , *J. Photochem. Photobiol. Chem.* 94 (1996) 191–203, [http://dx.doi.org/10.1016/0010-6030\(95\)04223-7](http://dx.doi.org/10.1016/0010-6030(95)04223-7).
- [37] P.J. Brown, D.S. Thomas, A. K hler, J.S. Wilson, J.-S. Kim, C.M. Ramsdale, H. Sirringhaus, R.H. Friend, Effect of interchain interactions on the absorption and emission of poly(3-hexylthiophene), *Phys. Rev. B* 67 (2003) 064203, <http://dx.doi.org/10.1103/physrevb.67.064203>.
- [38] S. Cook, A. Furube, R. Katoh, Analysis of the excited states of regioregular polythiophene P3HT, *Energy Environ. Sci.* 1 (2008) 294–299, <http://dx.doi.org/10.1039/B805643A>.
- [39] J. Piris, T.E. Dykstra, A.A. Bakulin, P.H.M. van Loosdrecht, W. Knulst, M.T. Trinh, J.M. Schins, L.D.A. Siebbeles, Photogeneration and ultrafast dynamics of excitons and charges in P3HT:PCBM blends, *J. Phys. Chem. C* 113 (2009) 14500–14506, <http://dx.doi.org/10.1021/jp904229q>.
- [40] S. Trotzky, T. Hoyer, W. Tuszynski, C. Lienau, J. Parisi, Femtosecond up-conversion technique for probing the charge transfer in a P3HT: PCBM blend via photoluminescence quenching, *J. Phys. Appl. Phys.* 42 (2009) 055105, <http://dx.doi.org/10.1088/0022-3727/42/5/055105>.
- [41] R.A. Cruz, T. Catunda, W.M. Facchinatto, D.T. Balogh, R.M. Faria, Absolute photoluminescence quantum efficiency of P3HT/CHCl<sub>3</sub> solution by Thermal Lens Spectrometry, *Synth. Met.* 163 (2013) 38–41, <http://dx.doi.org/10.1016/j.synthmet.2012.12.018>.